J Nanostruct 13(1): 66-75, Winter 2023

RESEARCH PAPER

Designing a Multi-Periodic Photonic Crystal with Adjustable Transmission Peak for Optical Filter Applications

Farideh Sadat Saeidi, Mehrdad Moradi *

Institute of Nanoscience and Nanotechnology, University of Kashan, Kashan, Iran

ARTICLE INFO

Article History:
Received 06 October 2022
Accepted 21 December 2022
Published 01 January 2023

Keywords:
1D-photonic crystal
Defect layer
Visible light filter
Thin film
Transfer matrix method

ABSTRACT

This paper deals with the effect of adding a TiO_2 thin film as a planar defect to a one-dimensional photonic crystal (PC) consisting of [Si/SiO_2] stacks. Theoretical calculations were carried out based on the 2×2 transfer matrix method (TMM) using MATLAB software in order to engineer the photonic band gap (PBG). The defect was considered as a variation in the refractive index, so that its presence in the structure leads to the breaking of the symmetry, creating a transmission peak (TP) in the forbidden band. In addition, the amplitude and location of TP can be shifted by changing physical parameters such as the functional wavelength range, thickness of layers, defect layer thickness, and angle of incidence. The results demonstrate that it is possible to arbitrarily engineer the transmission spectrum by changing the aforementioned parameters. Finally, two gaps are induced in the visible and infrared wavelength bands using an innovative and relatively symmetric structure. Through simple calculations, the location of the TPs can be appropriately engineered and adjusted. Importantly, $[Si/SiO_2]^3/TiO_2/[Si/SiO_2]^3/Si_3N_4$ PC structure with three adjustable TPs is designed, which can be used for band pass filter applications.

How to cite this article
Saeidi F S., Moradi M. Designing a Multi-Periodic Photonic Crystal with Adjustable Transmission Peak for Optical Filter Applications. J Nanostruct, 2023; 13(1):66-75. DOI: 10.22052/JNS.2023.01.008

INTRODUCTION

One-dimensional photonic crystals (1D-PCs) have been a hot topic in optical physics over the past two decades [1-5]. The 1D-PCs are a periodic structure created from distinct refractive indices of dielectrics. Refractive index periodicity leads to the formation of forbidden bands, called photonic band gaps (PBGs), controlling the propagation of light in specific wavelength ranges [6-8]. Also, the alternation of the forbidden band can be broken by entering a defect in PC [9], namely, the generation gap. Defects make the light pass through narrowband wavelengths in the forbidden band, which is known as the defect mode. In comparison with two-dimensional (2D) photonic crystals [10-12], one-dimensional (1D) photonic crystals are the most straightforward in their geometry and handling, allowing for controlling the properties of these structures and studying the influence of various physical parameters such as the layers order, number of periods, thickness of layers, defect layer thickness and the angle of incident [13-15]. Recently, there has been an increasing interest in 1D-PCs due to their capability to control and localize light [16-17], providing important consequences for designing waveguides, optical filters and omnidirectional mirrors [18-21]. An optical filter that operates as a Bragg mirror can

* *Corresponding Author Email: m.moradi@kashanu.ac.ir*

This work is licensed under the Creative Commons Attribution 4.0 International License.
To view a copy of this license, visit http://creativecommons.org/licenses/by/4.0/.

pass a range of wavelengths of light, while also blocking all other wavelengths. The laser eye protection is one of the most important optical filters used [22-24]. There are multiple ways for designing such filters including the use of polymer coatings [25], absorptive glass [26] and 1D-PC [22-24]. Many theoretical and numerical methods have been developed to understand and design 1D-PC structures. Among them, the plane wave expansion method (PWEM) [27], finite-difference time-domain (FDTD) [28-29], and transfer-matrix method (TMM) [30-35] have become popular.

In this paper, 1D-PCs consisting of $[Si/SiO_2]^6$ stacks on the Si_3N_4 substrate are designed, where SiO_2 and Si layers act as the low and high refractive index media, respectively. This structure can induce constructive and destructive interference due to the difference in refractive index among the materials. The SiO_2, Si and Si_3N_4 thin films are chosen in a way to provide minimum absorption in the visible wavelength region [36-37, 39]. Since the number of layers is selected in a long wavelength region (thus preventing the crystal from passing the light), the resulting filter has a low transmission, and is suitable to be used as an eye protection filter. A method of transferring matrix is then employed to determine the impact of defects (e.g., TiO_2), functional wavelength, defect layer thickness, and angle of incident on the optimization of 1D-PCs.

THEORETICAL FORMALISM

Calculating the reflectance and transmittance of the periodic multilayered structure is accomplished using the transfer matrix method. In this regard, the characteristic matrix corresponding to one stack is initially calculated and then distributed to a PC. The incident beam on the interface is split into two waves: a transmitted wave proceeding into the second layer and a reflected wave propagating back into the first layer (Fig. 1).

$$E_{i,j-1} = a\, e^{+i(k_{j-1}\cdot r-\omega t)} \qquad E_{t,j-1} = c\, e^{+i(k_j\cdot r-\omega t)} \quad (1)$$

$$E_{r,j-1} = b\, e^{-i(k_{j-1}\cdot r-\omega t)} \qquad E_{r,j} = d\, e^{-i(k_j\cdot r-\omega t)} \quad (2)$$

Where $E_{i,j-1}$ is the incident wave, $E_{r,j-1}$is the reflected wave from the dielectric of j-1th layer, $E_{t,j-1}$is the transmitted wave, and $E_{r,j}$ is the reflected wave from the dielectric of jth layer. The parameters a and c are amplitude of the incident and transmitted components, respectively. The parameters b and d indicate amplitude of the reflected components. Moreover, K_j is the wavenumber of the jth layer Kj=2πnj/λ. According to the boundary conditions (Eq. 3), when the free charge density or current density in the dielectric is 0, the tangential components of the resultant electric field are continuous across the interface as given by Eq. (4):

$$E_1^{\parallel} - E_2^{\parallel} = 0 \qquad \frac{B_1^{\parallel}}{\mu_1} - \frac{B_2^{\parallel}}{\mu_2} = 0 \quad (3)$$

$$E_{i,j-1} + E_{r,j-1} = E_{t,j-1} + E_{r,j} \quad (4)$$

$$a + b = c + d \quad (5)$$

Similarly, all tangential magnetic field components are also continuous, so that one

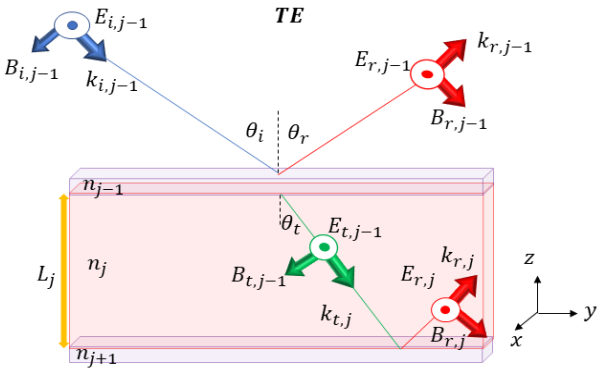

Fig. 1. Light propagation in multi-layer structure for TE mode. $E_{i,j-1}$, $B_{i,j-1}$, $E_{r,j-1}$, $B_{r,j-1}$, $E_{t,j-1}$, $B_{t,j-1}$ are the incident, reflected and transmitted waves from the dielectric of j-1th layer, respectively, $E_{r,j}$ and $B_{r,j}$ are the reflected waves from the dielectric of jth layer.

CC BY

obtains the following equations from |B|= n/c |E|:

$$n_{j-1}\,E_{i,j-1} - n_{j-1}\,E_{r,j-1} = n_j\,E_{t,j-1} - n_j\,E_{r,j} \quad (6)$$

$$n_{j-1}(a-b) = n_j(c-d) \quad (7)$$

These formulations relate the field components of the first boundary to those at the next boundary, and can be written in the matrix form as follows:

$$\begin{pmatrix} 1 & 1 \\ k_{j-1} & -k_{j-1} \end{pmatrix}\begin{pmatrix} a \\ b \end{pmatrix} = \begin{pmatrix} 1 & 1 \\ k_j & -k_j \end{pmatrix}\begin{pmatrix} c \\ d \end{pmatrix} \quad (8)$$

Accordingly, the transfer matrix of the j[th] layer, A_j, is expressed as follows for TE and TM modes by Eqs. (9) and (10), respectively:

$$A_j = \begin{bmatrix} 1 & 1 \\ k_j cos\theta_j & -k_j cos\theta_j \end{bmatrix} \quad (9)$$

$$A_j = \begin{bmatrix} cos\theta_j & cos\theta_j \\ k_j & -k_j \end{bmatrix} \quad (10)$$

The effect of propagation through a layer of index n_j, and thickness L_j is captured by the propagation matrix:

$$D_j = \begin{bmatrix} e^{-ik_jL_j} & 0 \\ 0 & e^{+ik_jL_j} \end{bmatrix} \quad (11)$$

Each layer of a multilayer has its own transfer matrix, and the total transfer matrix is the product of individual transfer matrices, which can be deduced as follows:

$$\begin{bmatrix} a \\ b \end{bmatrix} = [A_0^{-1}(A_1D_1A_1^{-1}A_2D_2A_2^{-1})^m\ A_S]\begin{bmatrix} c \\ d \end{bmatrix} \quad (12)$$

$$\begin{bmatrix} a \\ b \end{bmatrix} = \begin{bmatrix} M_{11} & M_{12} \\ M_{21} & M_{22} \end{bmatrix}\begin{bmatrix} c \\ d \end{bmatrix} \quad (13)$$

where air is denoted as 0, and the substrate is S. When the electromagnetic field propagates, it will produce a different phase ϕ between the reflected or transmitted waves, leading to interference effects, while also forming the PBG or TP. The reflectance and transmittance coefficients of the PC are provided with the elements of the transfer matrix as follows:

$$r = \frac{M_{21}}{M_{11}},\ t = \frac{1}{M_{11}} \quad (14)$$

Finally, the reflection and transmission parameters of a 1D-PC can be calculated using the following formula [30-35]:

$$T = \frac{n_s cos\theta_s}{n_0 cos\theta_0}|t|^2 = \frac{n_s cos\theta_s}{n_0 cos\theta_0}\left|\frac{1}{M_{11}}\right|^2, R = |r|^2 = \left|\frac{M_{21}}{M_{11}}\right|^2 \quad (15)$$

Fig. 2 shows the schematic of 1D-photonic crystal structure with Si/SiO_2 as stacks and TiO_2 as the defect. Here, Si and SiO_2 denote the high index and low index materials, respectively. Also, the number of the repetition for the basic structure is 6. The thicknesses of Si and SiO_2 thin films are L_1 and L_2, respectively.

RESULTS AND DISCUSSION

A 1D-PC consisting of $[Si/SiO_2]^m/Si_3N_4$ stacks is simulated where Si_3N_4 is the substrate, and Si and SiO_2 are thin films with high and low refractive indexes, respectively. At the start of the simulation, a functional wavelength (FW) is

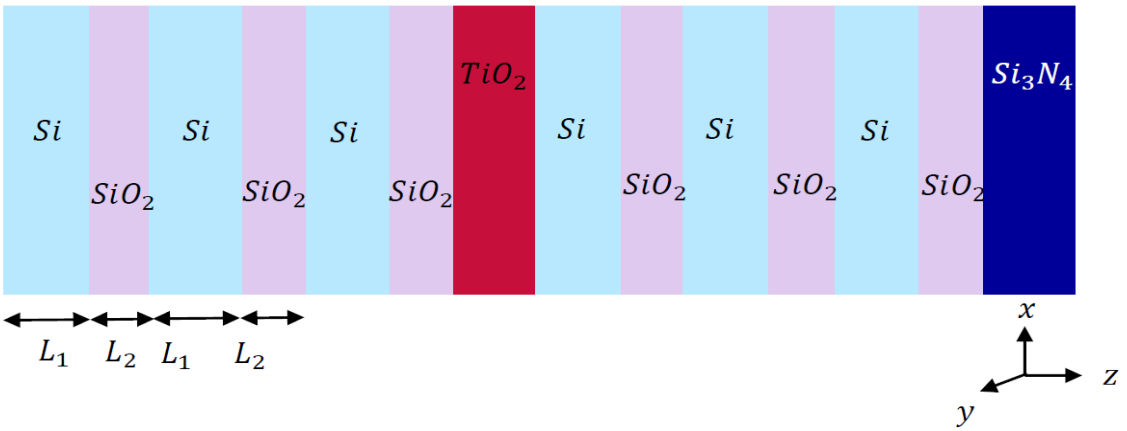

Fig. 2. The schematic of 1D-photonic crystal structure with Si/SiO_2 as stacks and TiO_2 as the defect.

CC BY

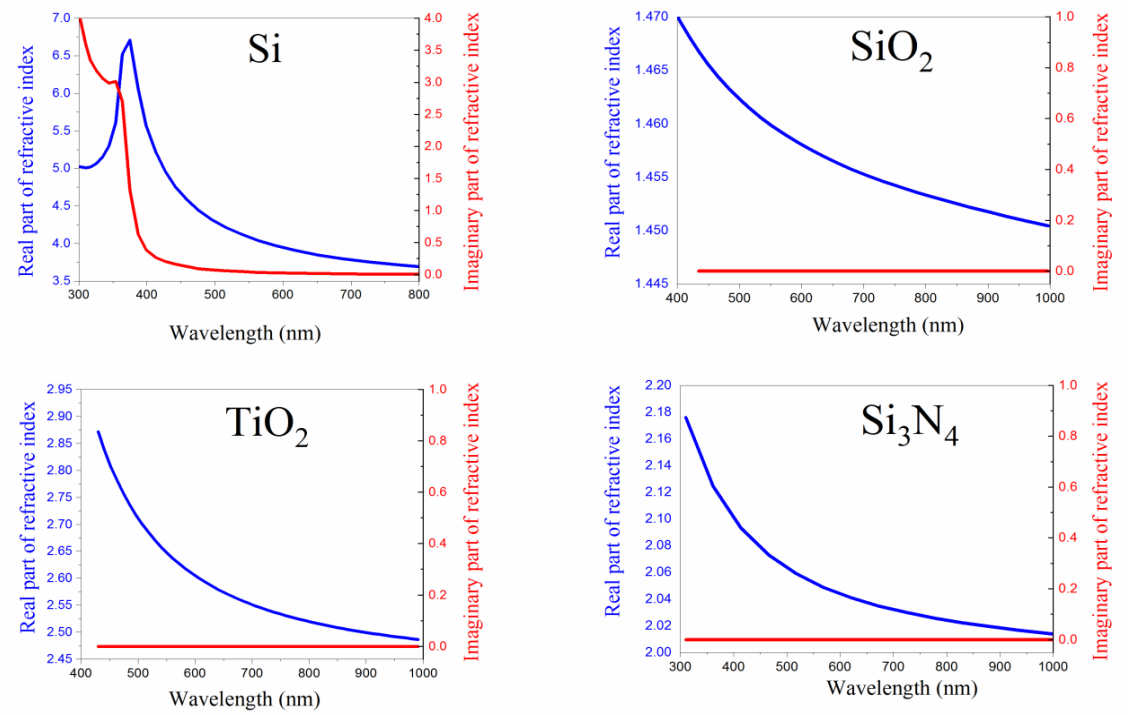

Fig. 3. Real part and imaginary part of refractive index for Si, SiO_2, TiO_2 and Si_3N_4.

selected to be 511 nm (in conformity with Copper Vapor laser) and layer thicknesses are then calculated. The wavelength is changed from 400 to 1000 nm in order to compute the transmission spectrum. Complex refractive indexes of thin films as a function of wavelength are extracted based on the literature [36-39] and are illustrated in Fig. 3. The thicknesses of all layers are obtained from $L= \lambda_F/(4n_j)$, where λ_F is the FW, being initially set to 511 nm. Since the refractive indexes of Si and TiO_2 are complex, their real parts are only taken into account for selecting the thicknesses. Therefore, thicknesses of Si_3N_4, Si, SiO_2 and TiO_2 thin films are selected to be 64.21, 37.37, 84.54 and 45.99 nm, respectively.

Fig. 4(a) displays the transmittance spectrum of the $[Si/SiO_2]^m/Si_3N_4$ structure. In this notation, the bracket demonstrates the layer pairs (the stack) and *m* denotes the number of stacks. The increase in the period number *m* results in the formation and growth of the width of the photonic forbidden band or PBG, blocking the transmission of photons or light energy in certain frequencies (transmittance less than 2). Fig. 4(b) represents the transmission spectra of $[Si/SiO_2]^6/Si_3N_4$ and $[SiO_2/Si]^6/Si_3N_4$ 1D-PC structures, indicating the importance and effect of the arrangement of Si and SiO_2 layers in the stacks. Since the only difference between the two structures is in the order of Si and SiO_2 thin films, obtaining similar transmission spectra is predictable and reasonable. Therefore, $[Si/SiO_2]^6/Si_3N_4$ structure is chosen arbitrarily.

In the following, TiO_2 layer is inserted as a defect layer, and sandwiched between three stacks of $[Si/SiO_2]$, resulting in $[Si/SiO_2]^3/TiO_2/[Si/SiO_2]^3/Si_3N_4$ structure. It is known that inserting a defect layer in a 1D-PC leads to the creation of a defect mode in its PBG [40-41]. Fig. 5 illustrates transmission spectra of the $[Si/SiO_2]^3/TiO_2/[Si/SiO_2]^3/Si_3N_4$ structure, which is calculated for FWs of 461 nm (Rhodamine 6G laser), 511 nm (Copper Vapor laser), 594 nm (Red He-Ne laser), 612 nm (Yellow He-Ne laser), 711 nm (NIR Laser Diodes), 811 nm (NIR Laser Diodes), and 911 nm (NIR Laser Diodes).

Fig. 5(a) indicates the occurrence of one transmission peak (TP) for the different FWs. Also, it is found that the TP shifts to longer wavelengths (i.e., a red shift) with increasing FW value. In order to investigate the effect of higher FWs on TP shift, transmission spectrum of $[Si/SiO_2]^3/TiO_2/[Si/SiO_2]^3/Si_3N_4$ PC is calculated for

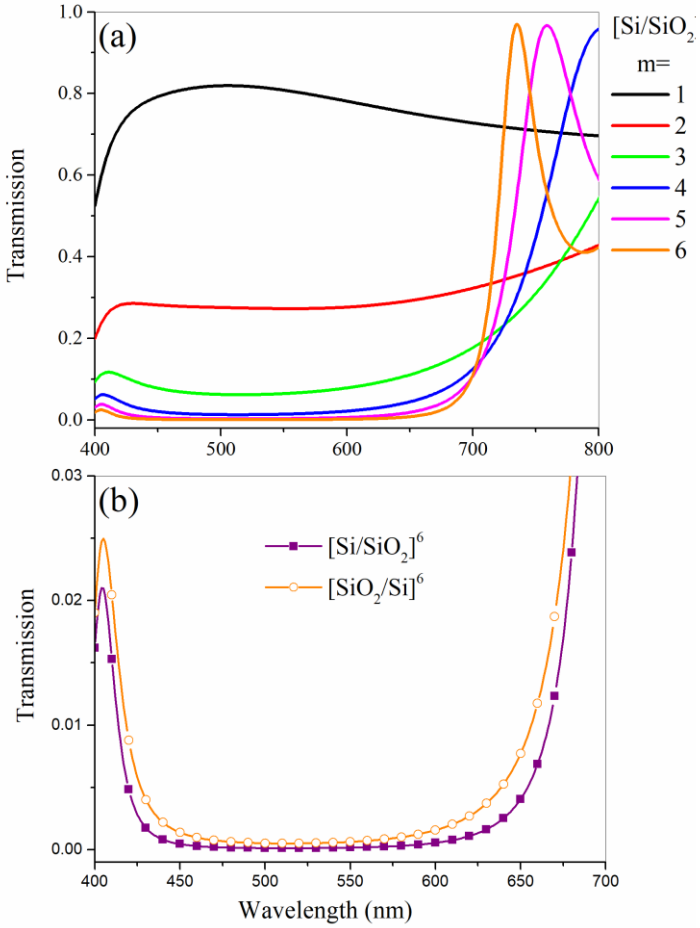

Fig. 4. (a). Transmittance spectrum of the $[Si/SiO_2]^m/Si_3N_4$ for m = 1, 2, 3, 4, 5, 6 (b). Transmission spectra of $[Si/SiO_2]^6/Si_3N_4$ and $[SiO_2/Si]^6/Si_3N_4$ 1D-PC structures.

FWs of 711, 811 and 911 nm, and the results are shown in Fig. 5(b). Note that, all layer thicknesses are calculated from the following formula: $L= \lambda_F/(4n)$, positioning the TP location exactly on the selected FW. However, in addition to a TP at 711 nm, there is a transmission region for FW = 711 nm whose average transmission is up to 80%, according to Fig. 5(b). For FW = 911 nm, there is also a TP at 911 nm and a transmission region at the wavelength ranges between 450-684 nm, as is shown with the dotted arrow. As a result, one can find that the location of the TP, the number of TPs, the PBG and the intensity of the transmitted light in Fig. 5(b) can be completely engineered and controlled. Table 1 shows that, as the FW increases, the maximum transmission and the PBGs width increase, whereas the width of the right PBG shows a noticeable change with the increase in FW.

According to the results of Figs. 5(a) and 5(b), one can change the PBG position with changing the thicknesses of all layers. However, we aim to change the position of PBG in a simpler manner, due to the defect layer thickness. To this end, the defect layer thickness is only changed from 20 to 100 nm, and the results obtained are shown in Fig. 6.

As can be seen, when the FWs of all layer thicknesses are fixed at 511 nm, and the thickness of the defect layer varies from 20 to 100 nm, the location of TP changes and can be divided into the two following regions: thicknesses between 20-70 nm where the position of TP is located between wavelengths of 438-590 nm, and thicknesses between 71-100 nm where the two TPs are located in the wavelength ranges of 618-

CC BY

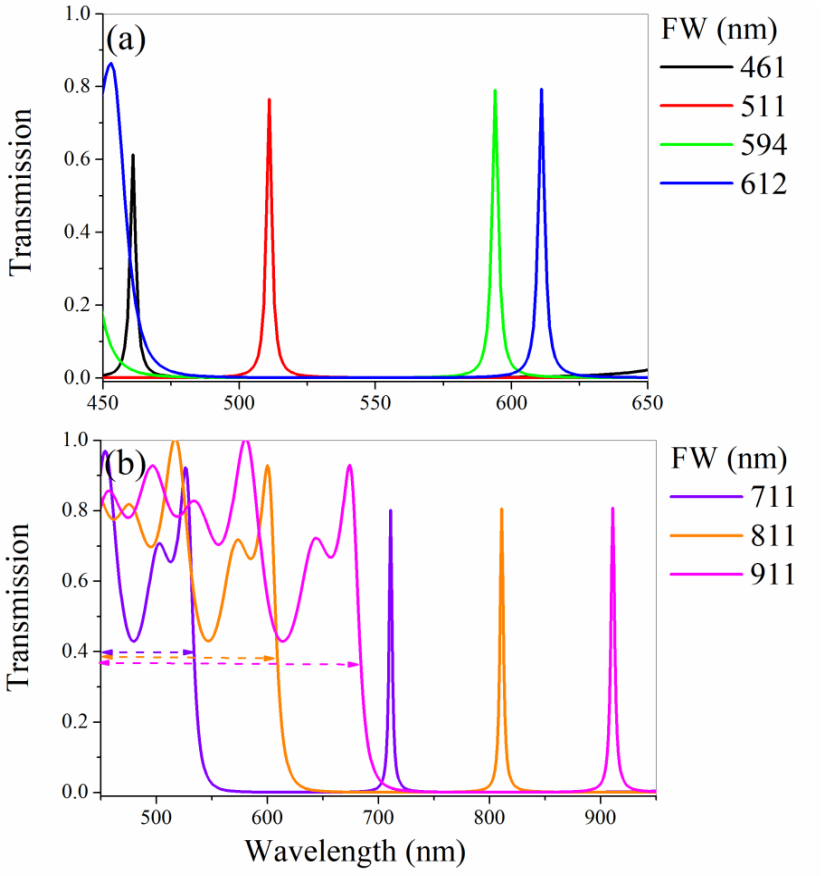

Fig. 5. Transmission spectra of $[Si/SiO_2]^3/TiO_2/[Si/SiO_2]^3/Si_3N_4$ PC calculated for: (a) FWs of 461, 511, 594 and 612 nm. (b) FWs of 711, 811 and 911 nm.

Table 1. TP location, maximum transmission and PBGs width. The dashed line indicates that there is no left PBG at FW 461 and 511 nm.

TP location (nm)	Maximum Transmission	Right PBG	PBG_R width (nm)	Left PBG	PBG_L width (nm)
461	0.61	(468-647)	179	-	-
511	0.76	(519-718)	199	-	-
594	0.79	(603-835)	232	(462-585)	123
612	0.79	(621-861)	240	(476-603)	127
711	0.80	(722-1001)	279	(553-701)	148
811	0.81	(823-1142)	319	(630-799)	169
911	0.81	(922-1284)	362	(707-898)	191

668 nm and 421-451 nm. In this way, we have to define two different equations to understand the relationship between the thickness of defect layer and the TP location. For thicknesses between 20-100 nm, the relationship between the selected thickness of defect layer and the location of TP can be calculated from the following equation #1: Y = 380.97 + 2.93 X. On the other hand, for thicknesses

CC BY

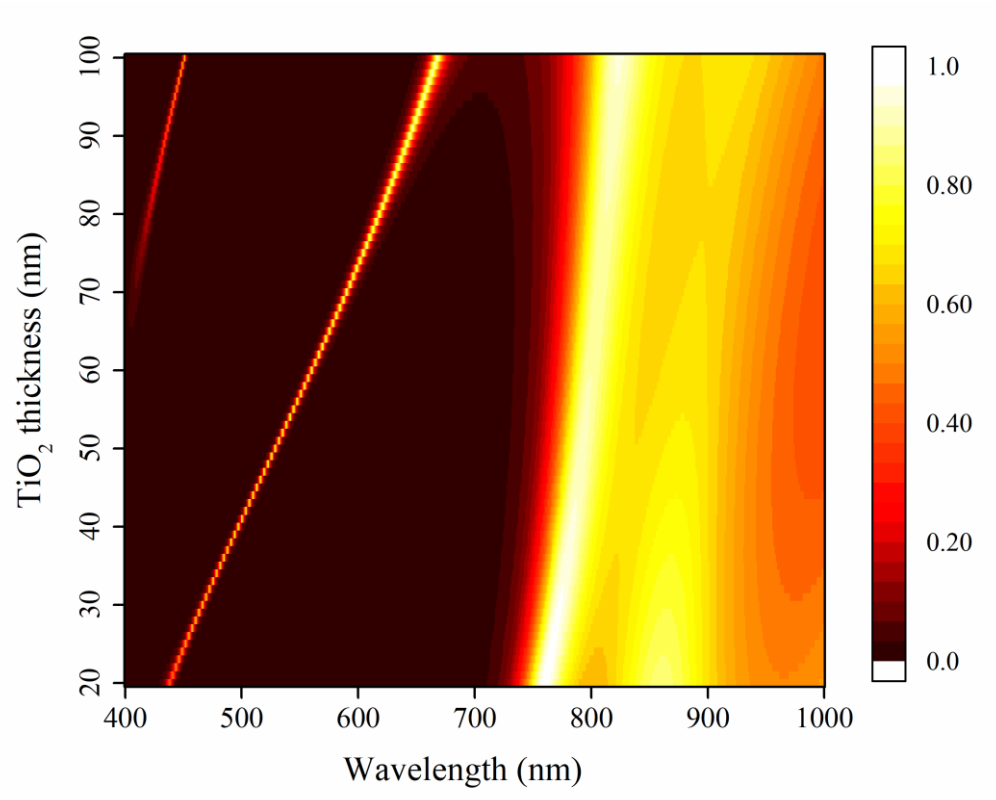

Fig. 6. Transmission spectra of $[Si/SiO_2]^3/TiO_2/[Si/SiO_2]^3/Si_3N_4$ PC as a function of wavelength and thickness of defect layer.

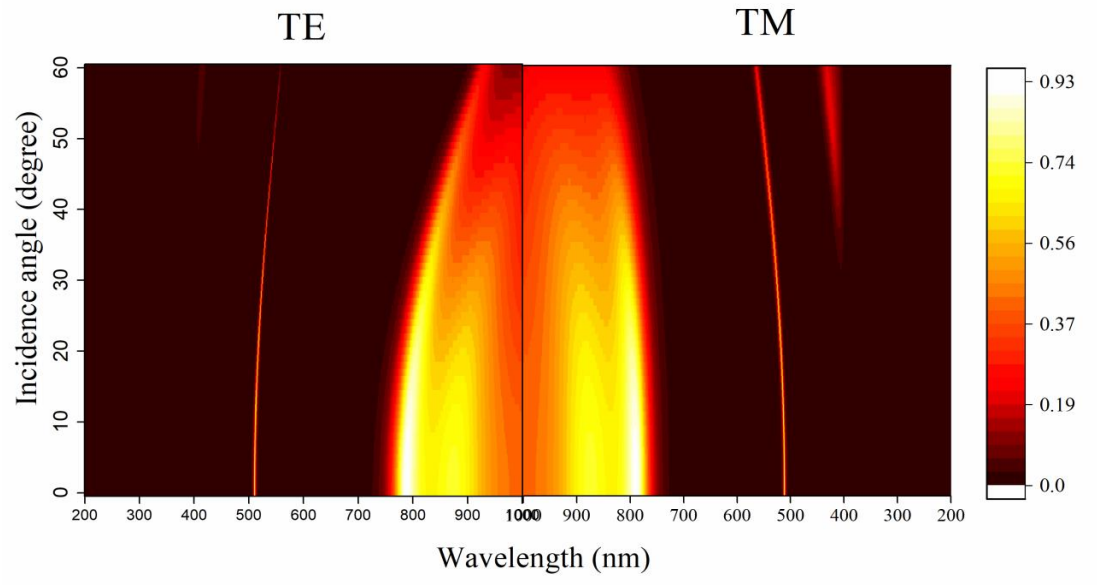

Fig. 7. Transmission spectra of $[Si/SiO_2]^3/TiO_2/[Si/SiO_2]^3/Si_3N_4$ PC as a function of wavelength and incidence angle for both TE and TM modes.

CC BY

between 71-100 nm, the relationship between the selected thickness and the location of the second TP can be calculated from the following equation #2: Y = 300.67 + 1.5 X. Using equations #1 and #2, it is possible to set the TP location on the desired thickness. For example, by using equation #1 and selecting the thickness of the defect layer to be 70 nm, it is possible to locate the TP at 590 nm. Therefore, this structure allows for locating the TP on any desired thickness. It should be noted that this ability is just possible for the structures whose stacks are the same on both sides of the defect layer.

Next, we analyze the effects of the incident angle on performance of the PCs. With increasing the incident angle from 0° to 60°, the TP location shifts to regions of longer wavelengths, and the TP height decreases. According to the results shown in Fig. 7, the TP height of the TE mode is 0.76 at 0°, 0.56 at 30°, and 0.1 at 60°. As well, the TP height of the TM mode is 0.57 at 30°, and 0.23 at 60°. This demonstrates that the incident angle affects the TP height, so that the TP height is maximum when the incident angle θ is 0°. It is also interesting to note that there is another TP at TM mode from 41-60 degrees, decreasing the TP height with the increase in the angle of incidence. In this case, the dependence of TP location and TP height on the incident angle is shown in Fig. 8.

From Figs. 5(a) and 5(b), putting the two structures together may lead to an optical filter with two or three TPs, leading to a so-called multi-optical filter. This arises from a transmission gap and a forbidden band for transmission in each structure. To verify this idea, two consecutive structures ($[Si/SiO_2]^3/TiO_2/[Si/SiO_2]^3$ structure with FW of 511 nm and $[Si/SiO_2]^3/TiO_2/[Si/SiO_2]^3/Si_3N_4$ structure with FW of 911 nm) along with the transmission of a merged structure as a function of wavelength are taken into consideration, and the calculated results are presented in Fig. 9. Evidently, the transmission is found to be possible only for the two aforementioned wavelengths, resulting from the combination of the two different transmissions of the consecutive structures. Note that the transmission is about zero for the rest of the spectrum. Hence, since the transmission of the two structures is below unity (< 1) at each FW,

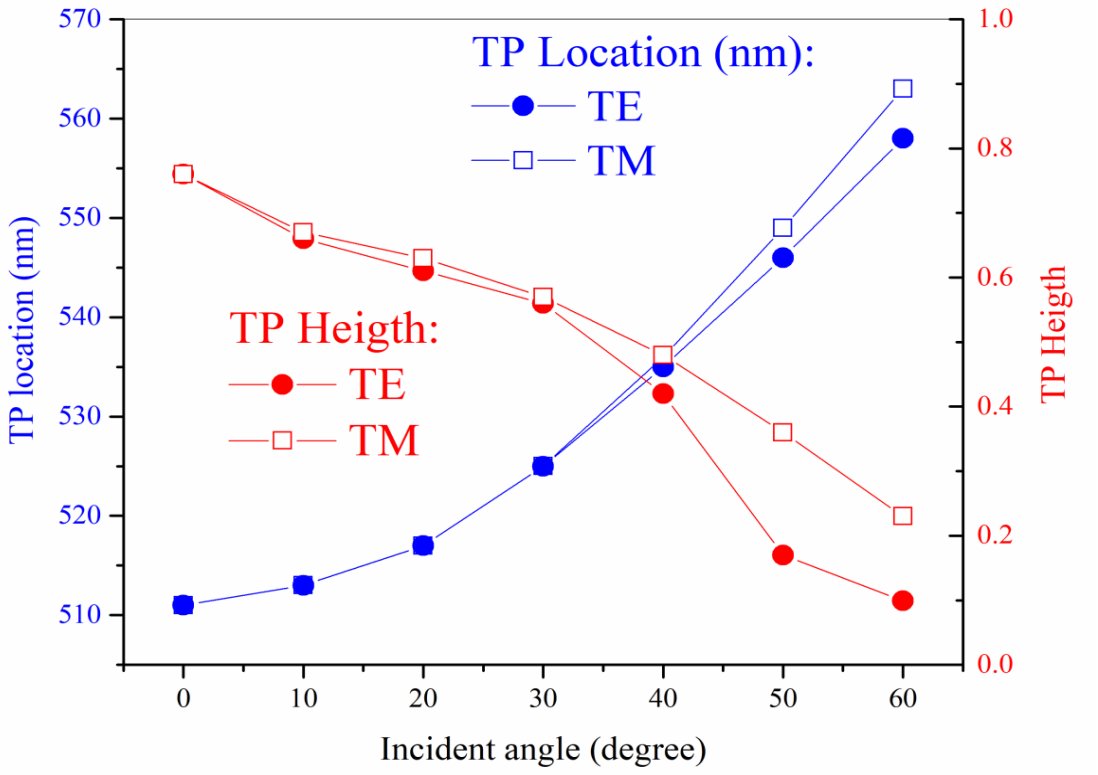

Fig. 8. The angle-dependent of TP location and TP height for both TE and TM modes with defect.

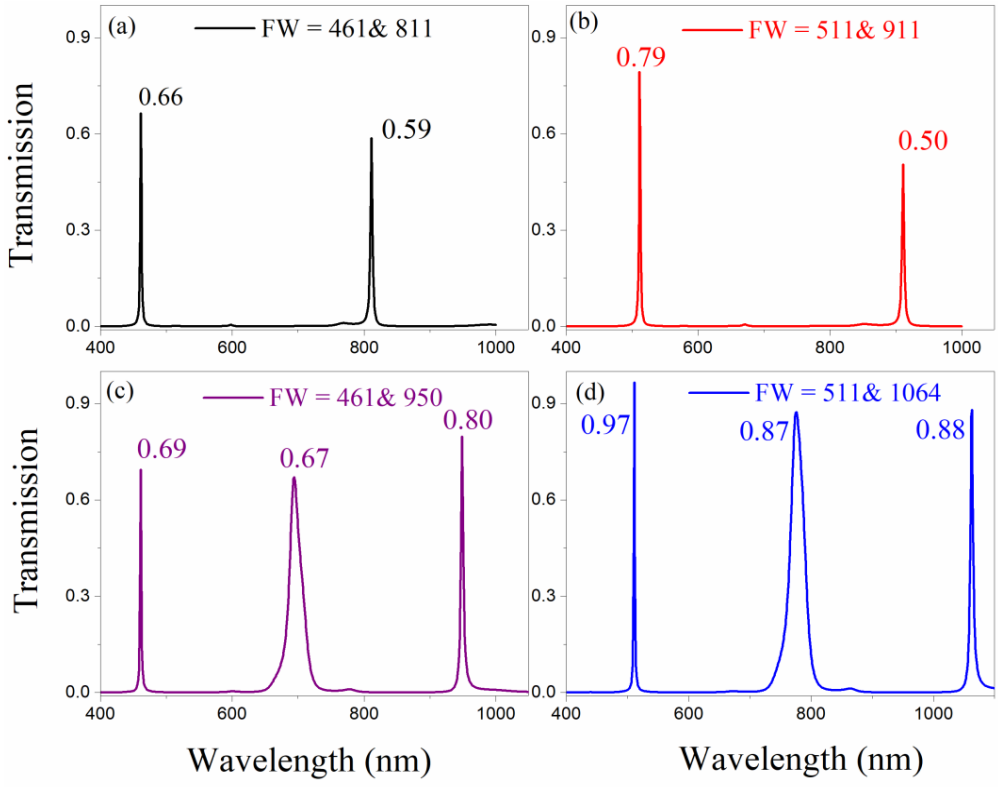

Fig. 9. Transmission spectra of $[Si/SiO_2]^3/TiO_2/[Si/SiO_2]^3/Si_3N_4$ PC for FWs of (a) 461 and 811 nm, (b) 511 and 911 nm and (c) 461 and 950 nm (d) 511 and 1064 nm.

it is reasonable to have an aggregate transmission of less than unity for their combined structure at each specific wavelength. In this case, the aggregate transmission for all TPs is less than 1.

On the other hand, three TPs are observed in wavelengths of 461, 694 and 949 nm for the combination of FWs = 461 and 950 nm. Also, three TPs are observed in wavelengths of 511, 776 and 1063 nm for the combination of FWs = 511 and 1064 nm. From an experimental standpoint, one can design a consecutive structure of $[Si/SiO_2]$ stacks to obtain the results of our simulations, thus forming an optical filter with three TPs.

CONCLUSION

The transfer matrix method was used to simulate the transmission spectrum in the 1D-PC consisting of $[Si/SiO_2]$ stacks. The results showed that the forbidden band can be broken, creating a TP by inserting a TiO_2 thin film as a defect. The simulation calculations indicated that the TP shifted toward longer wavelengths with increasing FW, positioning the TP location exactly on the selected FW. By fixing the FW of all layer stacks and changing thickness for the defect layer, the location of TP was shown to be divided into two regions, thus allowing for locating the TP at each desired thickness. Moreover, the relationship between selected thickness and the TP location was discussed. The incident angle affected the TP location, and the TP height. Finally, a filter with two or three TPs was obtained by putting two stacked structures together, being applicable for designing and fabricating optical filters.

CONFLICT OF INTEREST

The authors declare that there is no conflict of interests regarding the publication of this manuscript.

REFERENCES

1. Wan B-F, Zhou Z-W, Xu Y, Zhang H-F. A Theoretical Proposal for a Refractive Index and Angle Sensor Based on One-Dimensional Photonic Crystals. IEEE Sens J. 2021;21(1):331-338.
2. Kaviani Baghbadorani H, Barvestani J. Sensing improvement of 1D photonic crystal sensors by hybridization of defect and Bloch surface modes. Applied Surface Science. 2021;537:147730.

CC BY

3. Wang H-h, Liu W-x, Ma J, Liang Q, Qin W, Lartey PO, et al. Design of (GO/TiO_2)N one-dimensional photonic crystal photocatalysts with improved photocatalytic activity for tetracycline degradation. International Journal of Minerals, Metallurgy and Materials. 2020;27(6):830-839.
4. Hamidi SM. Optical and magneto-optical properties of one-dimensional magnetized coupled resonator plasma photonic crystals. PhPl. 2012;19(1):012503.
5. Shiveshwari L, Awasthi SK. Band gap characteristics of 1D static and moving photonic crystal. Physica B: Condensed Matter. 2020;597:412360.
6. Yablonovitch E. Inhibited Spontaneous Emission in Solid-State Physics and Electronics. Physical Review Letters. 1987;58(20):2059-2062.
7. John S. Strong localization of photons in certain disordered dielectric superlattices. Physical Review Letters. 1987;58(23):2486-2489.
8. Bananej A, Hamidi SM, Li W, Li C, Tehranchi MM. A flexible design for one-dimensional photonic crystals with controllable photonic bandgap width. Optical Materials. 2008;30(12):1822-1827.
9. Ansari N, Mirbaghestan K. Design of Wavelength-Adjustable Dual-Narrowband Absorber by Photonic Crystals With Two Defects Containing MoS_2 Monolayer. Journal of Lightwave Technology. 2020;38(23):6678-6684.
10. Vahdati A, Parandin F. Antenna Patch Design Using a Photonic Crystal Substrate at a Frequency of 1.6 THz. Wireless Personal Communications. 2019;109(4):2213-2219.
11. Karkhanehchi MM, Parandin F, Zahedi A. Design of an all optical half-adder based on 2D photonic crystals. Photonic Network Communications. 2016;33(2):159-165.
12. Parandin F, Kamarian R, Jomour M. Optical 1-bit comparator based on two-dimensional photonic crystals. Applied Optics. 2021;60(8):2275.
13. Dalmis R, Ak Azem NF, Birlik I, Çelik E. SiO_2/TiO_2 one-dimensional photonic crystals doped with Sm and Ce rare-earth elements for enhanced structural colors. Applied Surface Science. 2019;475:94-101.
14. Dadoenkova NN, Dadoenkova YS, Panyaev IS, Sannikov DG, Lyubchanskii IL. One-dimensional dielectric bi-periodic photonic structures based on ternary photonic crystals. Journal of Applied Physics. 2018;123(4):043101.
15. Panyaev IS, Yafarova LR, Sannikov DG, Dadoenkova NN, Dadoenkova YS, Lyubchanskii IL. One-dimensional multiperiodic photonic structures: A new route in photonics (four-component media). Journal of Applied Physics. 2019;126(10):103102.
16. Dubey RS, Ganesan V. Fabrication and characterization of TiO_2/SiO_2 based Bragg reflectors for light trapping applications. Results in Physics. 2017;7:2271-2276.
17. Saeidi FS, Moradi M. A new route to designing a one-dimensional multiperiodic photonic crystal with adjustable photonic band gap and enhanced electric field localization. Optics Communications. 2021;493:126999.
18. Torrijos-Morán L, Griol A, García-Rupérez J. Slow light bimodal interferometry in one-dimensional photonic crystal waveguides. Light: Science & Applications. 2021;10(1).
19. Gahef T, Bouazzi Y, Kanzari M. Omnidirectional mirror at 1.3 and 1.55 µm for optical fiber communication by specific deformation of Bragg reflector. OQE. 2017;49(3).
20. Sathyadevaki R, Raja AS, sundar DS. Photonic crystal-based optical filter: a brief investigation. Photonic Network Communications. 2016;33(1):77-84.
21. Zaghdoudi J, Kanzari M. One-dimensional photonic crystal filter using a gradient-index layer. Optik. 2018;160:189-196.
22. Ahmed K, Khan AN, Rauf A, Gul A, Aslam M. Design and development of laser eye protection filter. Journal of Physics: Conference Series. 2013;439:012023.
23. Chen M, Li C, Xu M, Wang W, Ma S, Xia Y. Eye-protection glasses against YAG laser injury based on the band gap reflection of one-dimensional photonic crystal. Optics & Laser Technology. 2007;39(1):214-218.
24. Swope CH, Koester CJ. Eye Protection against Lasers. Applied Optics. 1965;4(5):523.
25. Jankovic J, Ogle BR, Zontek TL, Biegalski MD, Hollenbeck SM, Wells TM. Suitability of polycarbonate safety glasses for UV laser eye protection. Journal of Chemical Health & Safety. 2016;23(2):29-33.
26. Elbashar YH, Rashad MM, Rayan DA. Protection Glass Eyewear Against a YAG Laser Based on a Bandpass Absorption Filter. Silicon. 2016;9(1):111-116.
27. Norton RA, Scheichl R. Planewave expansion methods for photonic crystal fibres. ApNM. 2013;63:88-104.
28. Arriaga J, Ward AJ, Pendry JB. Order-N photonic band structures for metals and other dispersive materials. PhRvB. 1999;59(3):1874-1877.
29. Kaburcuk F, Duman Ç. Analysis of light scattering from anisotropic particles using FDTD method. JMOp. 2019;66(18):1777-1783.
30. Ben Ali N, Dhasarathan V, Alsaif H, Trabelsi Y, Nguyen TK, Bouazzi Y, et al. Design of output-graded narrow polychromatic filter by using photonic quasicrystals. Physica B: Condensed Matter. 2020;582:411918.
31. Esmaeilzadeh B, Moradi M, Jahantigh F. An investigation of magneto-optical Kerr effect signal by optical cavity in [Glass/Co/ZnS] structure. Journal of Magnetism and Magnetic Materials. 2018;460:207-212.
32. Joannopoulos JD, Johnson SG, Winn JN, Meade RD. Photonic Crystals: Princeton University Press; 2011 2011/10/30.
33. Esmailzadeh B, Moradi M. Enhancement of Kerr Signal in Co Thin Films Incorporating Ag Nanoparticles Surrounded by TiO_2. Journal of Superconductivity and Novel Magnetism. 2017;31(5):1483-1488.
34. Luque-Raigon JM, Halme J, Miguez H. Fully stable numerical calculations for finite one-dimensional structures: Mapping the transfer matrix method. Journal of Quantitative Spectroscopy and Radiative Transfer. 2014;134:9-20.
35. Mosaddeghian M, Moradi M. Establishing a Correction Factor for Oblique Angle Deposition and Its Verification by the Magneto-Optical Kerr Effect. Journal of Superconductivity and Novel Magnetism. 2021;34(3):865-873.
36. Tan CZ. Determination of refractive index of silica glass for infrared wavelengths by IR spectroscopy. Journal of Non-Crystalline Solids. 1998;223(1-2):158-163.
37. Aspnes DE, Studna AA. Dielectric functions and optical parameters of Si, Ge, GaP, GaAs, GaSb, InP, InAs, and InSb from 1.5 to 6.0 eV. PhRvB. 1983;27(2):985-1009.
38. DeVore JR. Refractive Indices of Rutile and Sphalerite. J Opt Soc Am. 1951;41(6):416.
39. Luke K, Okawachi Y, Lamont MRE, Gaeta AL, Lipson M. Broadband Mid-Infrared Frequency Comb Generation in a Si_3N_4 Microresonator. CLEO: 2015: OSA; 2015.
40. Moradi M, Alisafaee H, Ghanaatshoar M. The Kerr effect enhancement in non-quarter-wave lossy magnetophotonic crystals. Physica B: Condensed Matter. 2010;405(21):4488-4491.
41. Ansari N, Mirbaghestan K. Design of Wavelength-Adjustable Dual-Narrowband Absorber by Photonic Crystals With Two Defects Containing MoS_2 Monolayer. Journal of Lightwave Technology. 2020 Aug 11;38(23):6678-6684.

CC BY